Chapter 2

Functional Alkoxysilane Mediated Controlled Synthesis of Prussian Blue Nanoparticles, Enabling Silica-Alginate Bead Development; Nanomaterial for Selective Electrochemical Sensing

2.1 INTRODUCTION

Prussian blue (PB) type metal complexes, collectively called metal hexacyanoferrates (MHCFs), have considerably been researched and achieved significant interest due to their important properties i.e., electrochemical (Karyakin, 2001; Karyakin et al., 2000), magnetic (Arun et al., 2013; Rogez et al., 2000; Ruiz et al., 2005), electrochromic (Ellis et al., 1981; Varshney et al., 2003), photophysical (Pyrasch and Tieke, 2001), electrocatalytic (Gotoh et al., 2007; Itaya et al., 1984; Kawamoto et al., U.S. Patent 20110268963 A1, November 3, 2011; Mažeikienė et al., 2011; Pandey, Indian Patent 64/DEL/2012, Jan 06, 2012; Zeng et al., 2008; Zhao et al., 2005). The structure of MHCFs resembles the NaCl-type lattice and containing two metal atoms or one metal atom in two different oxidation states (Itaya et al., 1982a). The metal atoms can be varied as desired for a particular application. Among different synthetic protocols used for the preparation of MHCFs,a single precursor synthetic method based on the dissociation of either $K_3[M(CN)_6]$ or $K_4[M(CN)_6]$ (M= Co, Fe, etc.) in surfactant-formed microemulsion systems (Cao et al.,

2005; Jia and Sun, 2007; Wu et al., 2006; Zhang et al., 2007) is more desirable for PB synthesis than the aforementioned traditional process comprising double precursor. The size of MHCFs plays an important role from an application point of view. The smaller or even nanoscale sizes improve the dispersibility of these MHCFs in a particular solvent. It helps in the processing of the material for thin film formation, studying the electrochromic behavior and composite preparation. To date, several methods are outlined for the controlled synthesis of Prussian blue nanoparticles (PBN) of different sizes and shapes (Durand et al., 2010; Johansson et al., 2005; Uemura and Kitagawa, 2003)) by optimizing the molar ratio of protector to the precursor. The control over the particle shape and size during PB synthesis is an important aspect that builds up nanoparticle properties as a function of size (Fernandez et al., 2010; Shen et al., 2009; Sun et al., 2005;Uemura et al., 2004).

To address these issues, works evolved from the previous contributions for preparation of noble metal and PBN, which incorporate the active role of functional alkoxysilanes, 3-aminopropyltrimethoxysilane (3-APTMS) (Pandey and Pandey, 2013b,c). It is further attempted to exclude silica content and facilitate PBN synthesis by the active role of tetrahydrofuran-hydroperoxide (THF-HPO), tetrahydrofuran (THF) with H_2O_2 (Pandey and Panday, 2016; Pandey and Pandey, 2014). The use of these reagents enabled the PBN nanogeometry between 16-50 nm. The essential challenge is to explore new synthetic protocols that permit the nanosized MHCFs synthesis in a controlled manner obtaining; (i) narrow size distribution due to size-dependent properties, (ii) protection against aggregation, and (iii) homogeneous dispersion of MHCFs in different solvents with a wide range of chemical composition. Consequently, a new synthetic approach that may allow controlling the PBN diameter to manifest the electrochemical behavior as a function of the size is attempted in the current research.

MHCFs has been recommended for the effective removal of cesium and thallium from natural waters (Sangvanich et al., 2010). Accordingly, efforts have been made to incorporate the MHCFs within porous-matrix like calcium alginate beads for cesium ion (Cs^+) removal (Vipin et al., 2013). The larger PB particles successfully entrap within porous calcium alginate beads, but a smaller one (1-20 nm) may be leached out during practical applications. Accordingly, it is desirable to control the porous morphology of calcium alginate beads that precisely allow encapsulation of smaller PBN within porous

matrix rendering it worthy for potential biomedical applications. The role of alkoxysilanes containing R-Si(OR)$_3$, along with calcium alginate precursor, may yield the formation of silica-alginate beads through the formation of Si-O-Si- linkage within the porous matrix of calcium alginate. Although, the finding reported earlier, (Pandey and Pandey, 2013c) describes the use of 3-APTMS to facilitate the direct conversion of potassium ferricyanide into PB. However, It is not homogeneous with calcium alginate precursor, which is a key point in deriving alginate beads. The current result reports the innovation on these lines justifying the role of another functional alkoxysilane, namely, 2- (3,4-epoxycyclohexyl)ethyltrimethoxysilane (EETMSi). It is found that EETMSi enables controlled conversion of potassium hexacyanoferrate into PBN. Besides, the resultant nanodispersion is homogeneous with alginic acid and appropriate for delivering silica-alginatebeads, which are reported herein.

Pyrogallol is a significant reagent useful as an antioxidant and scavenger of reactive oxygen species (Alanko et al., 1999; Lambert et al., 2007) and free radicals (Rice-Evanset al., 1996; Yokozawa et al., 1998). The sensing of pyrogallol is a consequential necessity for chemical, environmental, clinical, and biological systems. Apart from several analyt-ical approaches e.g; chemiluminescence (Chen and Bai, 2008; Zhang and Zheng, 2006), fluorescence (Rao et al., 2017) and GC-MS (Tor et al., 1996), electrochemical approach for pyrogallol detection has received significant attention by means of CuHCF modified graphite paste electrode (Pandey and Pandey, 2013a). Since it also undergoes direct oxidation at the bare surface, which is susceptible to the nature of electrode materials, accordingly selectivity in electrochemical pyrogallol sensing has been a challenging task which is undertaken in current research.

The present finding demonstrates the influence of EETMSi that provides the facile and size-controlled synthesis of PB classified into small-sized (8 nm), medium-sized (17 nm), and large-sized (26 nm) nanoparticles and has interesting size-dependent peroxidase-like activity. Moreover, it derives even silica-alginate beads introducing the controlled pores, suitable for encapsulation of PBN (8 nm) along with justifying selective electrochemical sensing of pyrogallol. PB beads further add valuable information as the mesoporous matrix could again be loaded with another suitable reagent, including redox enzyme for selective applications. The findings on these lines are reported in this investigation.

2.2 EXPERIMENTAL

2.2.1 Materials

2-(3,4-epoxycyclohexyl)ethyltrimethoxysilane (EETMSi) with 97.0 % assay and cyclohexanone (99.8 % assay) were obtained from Pubchem. Graphite powder (particle size 1-2 μm), Nujol oil (density 0.838 g mL^{-1}) and o-dianisidine (99.8 % assay) were obtained from Sigma-Aldrich Chemical Co. India. Potassium ferricyanide (99.0 % assay) and hydrogen peroxide (H_2O_2) were purchased from Merck, India. All other chemicals used were obtained from the commercial source and were of analytical grade. Double distilled water was used in all experiments.

2.2.2 EETMSi mediated synthesis of PBN

The typical procedure of PBN synthesis involves, the mixing of optimum concentration of EETMSi and an aqueous solution of potassium ferricyanide followed by the addition of tetrahydrofuran hydroperoxide (THF-HPO) under stirring condition. The resulting green coloured solution was allowed to stand in an oven at 60°C for 3-5 hours to yield deep blue PBN homogeneous suspension. It was initially purified by solvent extraction using ethyl acetate. Different-sized PBN was obtained through the use of varying content (0.03 to 0.12 M) of EETMSi (5 μl) with a constant amount of potassium ferricyanide (0.1 M, 50μl) and THF-HPO (1.0 M, 40 μl).

2.2.3 Fabrication of PBN encapsulated silica-alginate beads

The PBN encapsulated silica-alginate beads were developed via adding PBN (100 μl, 10 mM) suspension to an aqueous solution of sodium alginate (50 μl, 2-2.5% w/v) under the stirring condition. Later the homogeneous nanosuspension was added dropwise from a glass syringe into 40 μl of an aqueous solution of calcium chloride under constant stirring at200 rpm. After 2 hours, the nanoparticle encapsulated silica-alginate beads were collected by filtration, washed several times with distilled water and ethanol.

2.2.4 Instrumentation

The UV-Vis absorption spectra of PBN was recorded using a Hitachi U-2900 spectrometer. TEM studies were performed using Hitachi 800 and 8100 electron microscopy (Tokyo,

Japan) with an acceleration voltage of 200 kV. IR spectra recorded on an ALFA FTIR Bruker-ATR, Ettington, Germany. Electrochemical experiments were accomplished on an electrochemical workstation model CHI660B, CH Instrument Inc., TX, in a three-electrode configuration with a working volume of 3 ml. An Ag/AgCl electrode served as a reference and counter electrode, respectively. All potentials given in the text are relative to the Ag/AgCl. The working electrode was a PBN-modified carbon paste electrode (CPE). The active paste of PBN was prepared by mixing 100 μl of PBN suspension with 60 mg spectroscopic grade graphite powder (particle size 1-2 μm), followed by ultrasonication for 30 minutes and left to dry in a vacuum oven for overnight. Electrode body used for electrochemical measurement has been purchased from Bioanalytical systems (West Lafayette, In (MF 2010). The composition of the typical active paste was found to be, graphite powder = 68%, w/w, and nujol oil = 28%, w/w, PBN = 4% w/w.

2.2.5 Kinetic assay

The steady-state kinetics were performed by varying the concentration of H_2O_2 (1-25 mM), at the fixed content of o-dianisidine dye (50 μM) and PBN catalyst (0.5 mM). The reaction was monitored in 2 ml phosphate buffer (0.1 M, pH$\sim$ 7.0), and the variation of absorbance has been observed at 490 nm in time scan mode. The kinetic parameters were calculated by fitting the absorbance data to the Michaelis-Menten equation as

$$V = V_{max}[C]/K_m + [C],$$

where V is the rate of conversion, V_{max} is the maximal reaction velocity, $[C]$ is the concentration of the substrate, and K_m is the Michaelis-Menton constant.

2.2.6 Catalytic activity of PBN as peroxidase

The peroxidase-like activity of as-synthesized PBN was determined spectrophotometrically by measuring the formation of an oxidized product of chromogenic o-dianisidine dye at 430 nm (E = 11.3 mM^{-1} cm^{-1}) using a Hitachi U-2900 spectrophotometer. The experiment was performed in 2 ml of 0.1 M phosphate buffer (pH$\sim$ 7.0) in the presence of an active catalyst PBN (1.2 mM), using o-dianisidine dye (50 μM) and varying concentration of H_2O_2 (1-25 mM) at room temperature.

2.2.7 Electrochemical sensing of H_2O_2

The modified electrode was used for detection of H_2O_2 in 0.1 M phosphate buffer containing 0.5 M KCl (pH~ 7). The cyclic voltammograms recorded before and after the addition of H_2O_2 at the scan rate of 0.01 Vs^{-1} between the potential range of −0.2 V to 0.5 V vs. Ag/AgCl.

2.2.8 Electrochemical oxidation of pyrogallol through PBN encapsulated silica-alginate beads

PBN encapsulated silica-alginate bead was used for pyrogallol oxidation in 0.1 M phosphate buffer containing 0.5 M KCl (pH~ 7). Beads were suspended in phosphate buffer placed in an electrochemical cell equipped with a glassy carbon working electrode, platinum counter electrode, and Ag/AgCl reference electrode. The differential pulse voltammetry (DPV) was recorded in different conditions at the scan rate of 0.001 V s^{-1} between the potential range of −0.2 V to 0.5 V vs. Ag/AgCl.

2.3 RESULT AND DISCUSSION

2.3.1 Effect of alkoxysilane on PBN synthesis

Role of functional alkoxysilanes like EETMSi and 3-glycidoxypropyltrimethoxysilane (3-GPTMS) have been examined for controlled reduction of noble metal cations into respective nanoparticles (Pandey et al., 1999b; Pandey and Chauhan, 2012; Pandey et al., 2017). Such findings directed us to extract their synthetic ability towards PBN formation using a single precursor potassium hexacyanoferrate. Surprisingly, EETMSi facilitated the synthesis of PB, including rapid seeding with controlled crystal growth to develop nano-size particles of multiple dimensions. Fig. 2.1 explains the typical results on EETMSi mediated formation of PBN based on UV-Vis spectroscopy. Fig. 2.1 shows absorption maxima at 420 nm (Curve-a), characteristics of potassium ferricyanide (Harish et al., 2011; Pandey and Pandey, 2013b). On the addition of EETMSi and THF-HPO, the yellow-coloured solution changed into green (image-b), indicating decrease in the absorption maxima (curve-b) due to dissociation of potassium ferricyanide (Fig. 2.1). The green suspension was kept in an oven at 60°C, later the colour was turned into deep blue

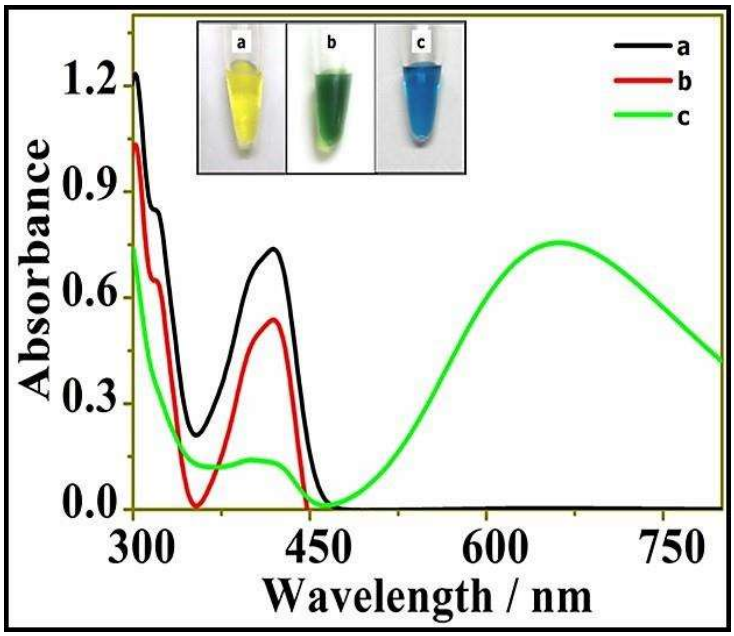

Figure 2.1: UV-Vis spectra of; (a) 0.1 M potassium ferricyanide (b) reaction mixture containing 0.1 M ferricyanide, and 1 M THF-HPO (c) reaction mixture containing 0.1 M ferricyanide, 1 M THF-HPO, and 0.03 M EETMSi after incubation at 60°C for 5 h. The inset shows the visual images (a,b,and c) of correspondings.

---

colour (image-c). The characteristics absorbance maxima close to 670 nm (curve-c), indicating the EETMSi mediated formation (Fig. 2.1) of PBN (Farah et al., 2013). The effect of both EETMSi and THF-HPO on conversion of potassium ferricyanide into PBN have been examined in different conditions through varying the concentration of one of reagent; THF-HPO/Potassium ferricyanide/EETMSi, while keeping other two constant. The changes in the absorbance maxima were recorded throughout the component variation and displayed in the Fig. 2.2, Fig. 2.3, and Fig. 2.4.

The results recorded in Fig. (2.2, 2.3 and 2.4) justify that optimum concentration of each reagent, i.e., THF-HPO/$K_3Fe(CN)_6$/EETMSi play crucial role to yield PBN. Subsequent investigation has been carried out to understand the effect of EETMSi in controlling the PBN size. The results based on transmission electron microscopy (TEM) justify the effect of same on PBN size. PBN prepared at three different concentrations of EETMSi i.e., 0.03 M for PBN-1 (Fig. 2.5A); 0.06 M for PBN-2 (Fig. 2.6A) and 0.12 M for PBN-3 (Fig. 2.7A), are quite spherical and uniformly distributed. The selected area

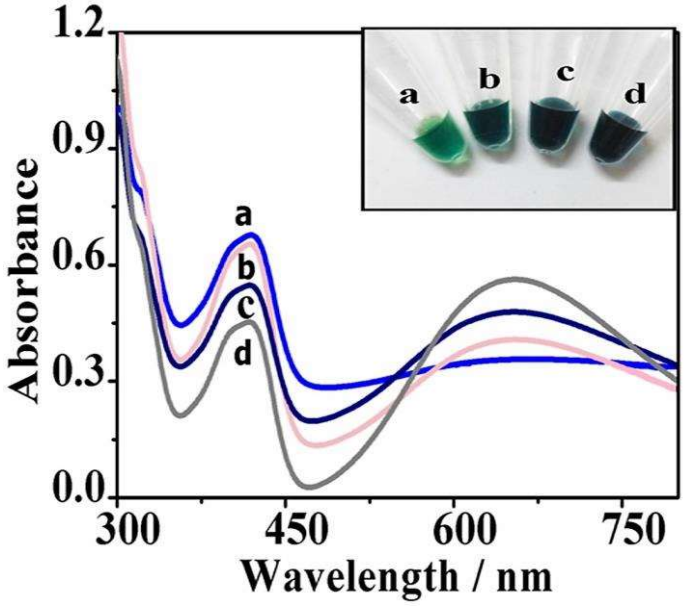

Figure 2.2: PBN formation, based on THF-HPO concentration variations; (a)1 M (b) 2 M (c) 3 M (d) 4 M, at constant ferricyanide (0.1 M) and EETMSi (0.03 M) content.

---

electron diffraction (SAED) pattern having Bragg spots making ring ((Fig. 2.5B, Fig. 2.6B, Fig. 2.7B)) evidently shows the polycrystalline nature of the PBN. Characteristically the different planes (111), (200), (220), (311), (222), (400), featured in above PBN is indexed to the face-centered cubic type of crystal lattice (Pandey and Panday, 2016; Zhuang et al., 2017). The resultant histograms (Fig. 2.8(A,B,C)) confirmed the average particles dimension ranges from 26 to 8 nm.

Effect of EETMSi concentration during PBN synthesis has further been evaluated based on zeta potential measurement. The appliance of suitable surfactants during nanoparticle synthesis is a convenient approach to prevent nanoparticles from aggregation (Gotoh et al., 2007). Measured zeta potentials as displayed in Fig. 2.9(A) are, −6 mV, −12 mV, −20 mV and −32 mV for PBN-0 (50 nm), PBN-1 (26 nm), PBN-2 (17nm) and PBN-3 (8 nm) respectively. Their corresponding negative signal indicated a negatively charged surface that recovered it without any further aggregation. The outcomes revealed that PBN-0 (synthesized in absence of EETMSi) possess very less zeta potential and hence less stability. On contrary, PBN-3 having more zeta value than others was

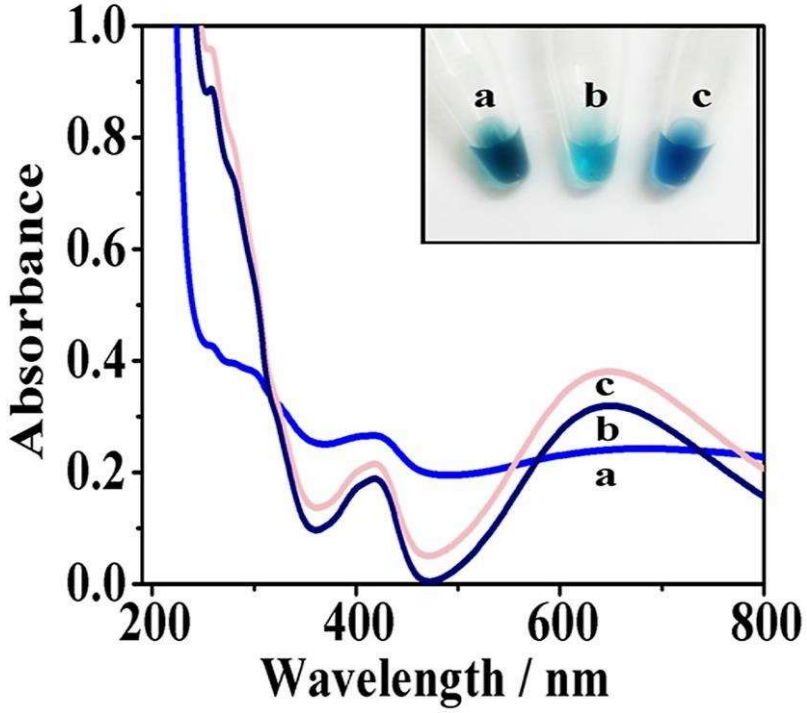

Figure 2.3: UV-Vis spectra of PBN synthesis, based on concentration variation of ferricyanide (a) 0.05 M (b) 0.1 M (c) 0.5 M, at constant THF-HPO (1 M) and EETMSi (0.03 M).

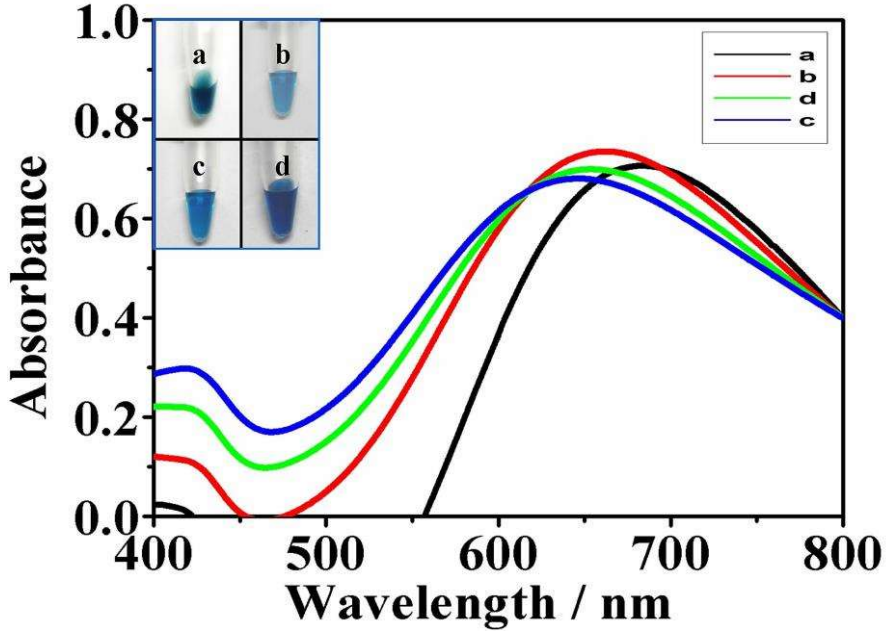

Figure 2.4: PBN formation based on concentration variation of EETMSi; (a) 0.0M (b) 0.03 M (c) 0.06 M and (d) 0.12 M, at constant THF-HPO (1 M) and ferricyanide (0.1 M).

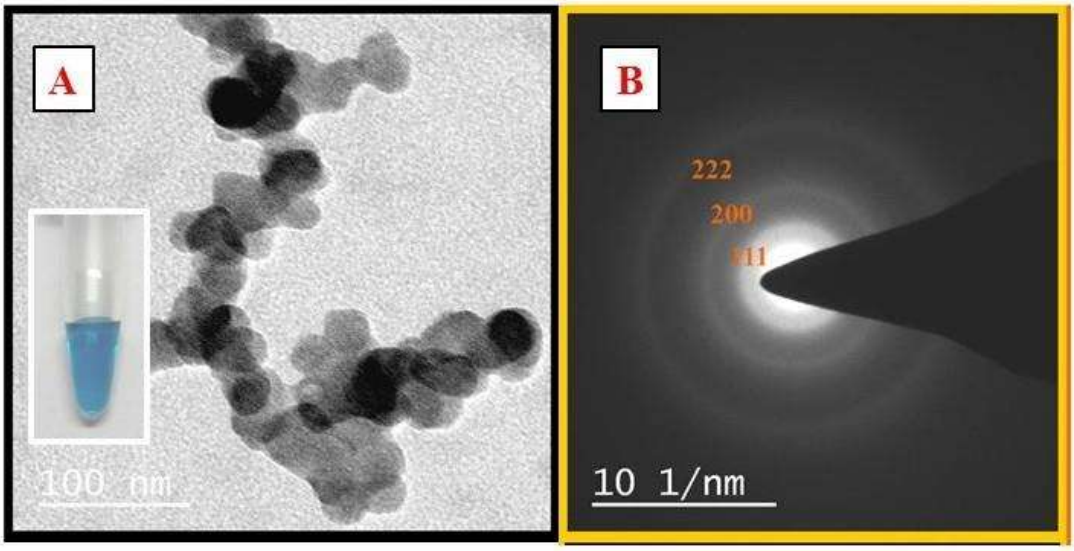

Figure 2.5: TEM and visual image of PBN-1 (A), SAED pattern (B) of corresponding nanoparticles (PBN-1).

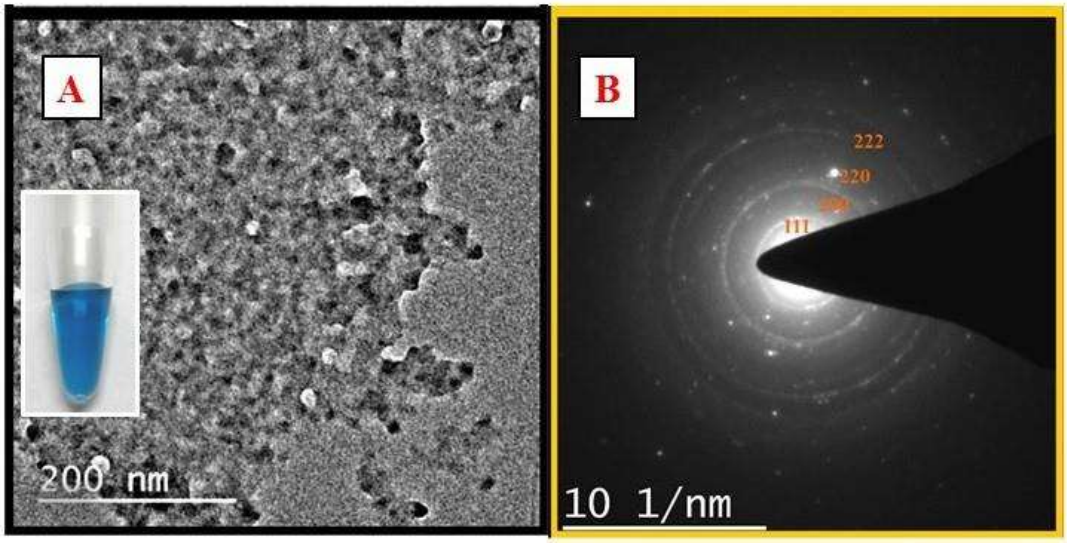

Figure 2.6: TEM and visual image of PBN-2 (A), SAED pattern (B) of corresponding nanoparticles (PBN-2).

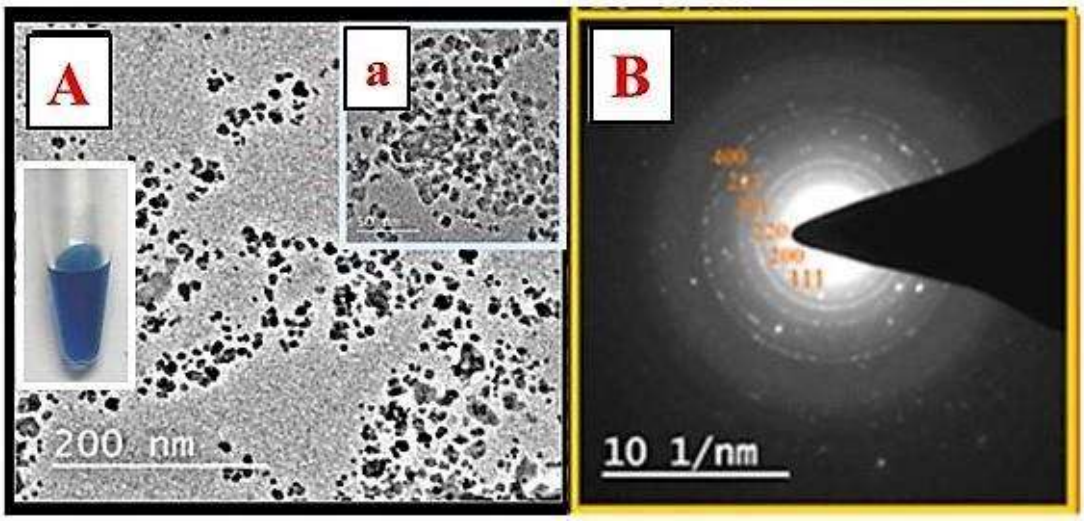

Figure 2.7: TEM and visual image of PBN-3 (A), SAED pattern (B) of corresponding nanoparticles (PBN-3). Inset (a) displays the nanoparticle at high magnification (scale bar of 50 nm).

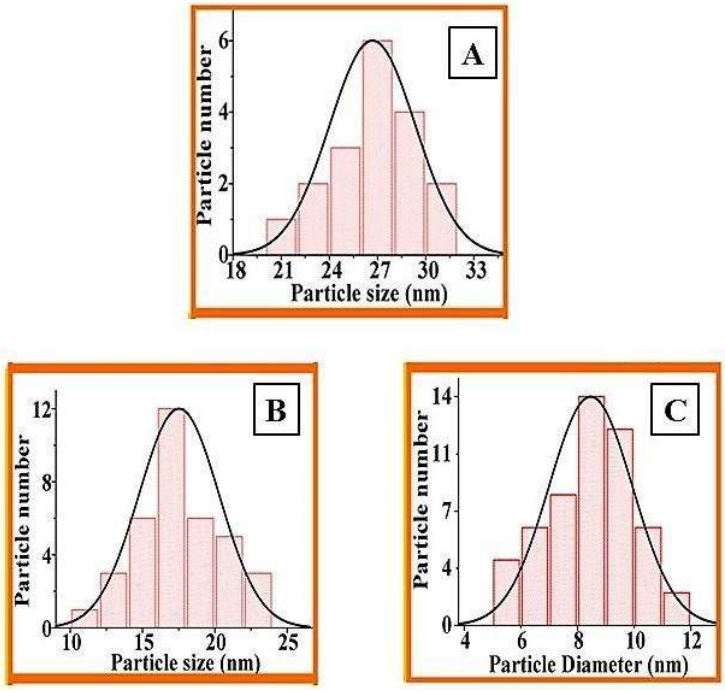

Figure 2.8: Bar histograms showing the particle size distribution of PBN-1 (A), PBN-2 (B), and PBN-3 (C).

undoubtedly due to the higher diffusion coefficient of smaller nanoparticles representing the better stability of the same.

The averaged diameter of PBN versus the EETMSi/Fe^{3+} ratio plot Fig. 2.9(B) revealed a gradual decrease in nanoparticle diameter on increasing EETMSi content. It is predictable that EETMSi might be playing a crucial role to suppress the crystal growth to yield smaller size nanoparticle at high concentration. But unexpectedly excessive EETMSi quantity unveiled adverse behavior and affected PBN catalytic and electrochemical activity owing to -Si-O-Si- linkage formation over the time. All these findings predict that fixed ratio of EETMSi and THF-HPO have probably the controls over particle nanogeometry and in turn to their activity.

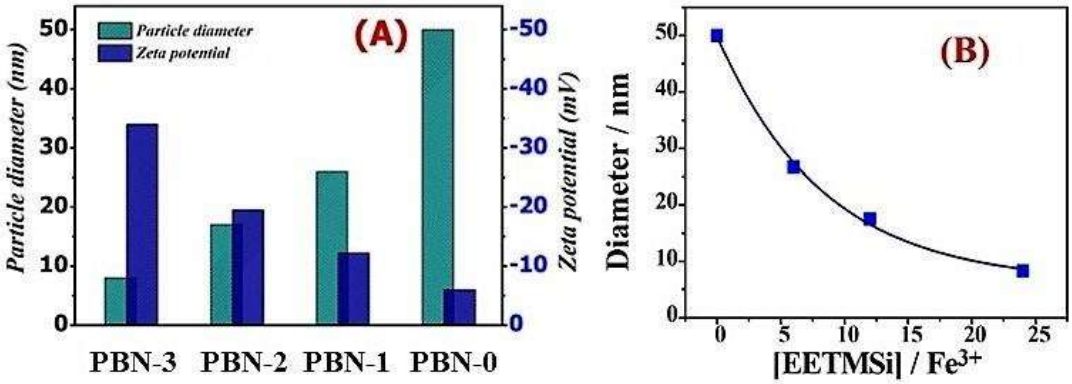

Figure 2.9: Dependence of zeta potential on particle diameter of PBN (A). Dependence of diameter of PBN with EETMSi /Fe^{+3} stoichiometric ratio (B).

2.3.2 Effect of EETMSi over charge transfer spectra of PBN

The intervalence charge transfer transition from Fe(II) carbon hole to Fe(III) nitrogen hole, revealed a peak at 680 nm in a spectrum, attributed for the blue colour of PBN (Robin, 1962). Variation in absorbance maxima may correspond to the different nano-geometry of PBN. Accordingly, PBN-1, PBN-2, and PBN-3 were examined based on these predictions. To precisely evaluate the role of EETMSi, PBN-0 was synthesized in the absence of EETMSi. The absorbance maxima recorded at different wavelengths of 681 nm, 668 nm, 657 nm, and 647 nm in UV-Vis spectra, as shown in Fig. 2.4, correspond to a

variable size of nanoparticles PBN-0, PBN-1, PBN-2, PBN-3, respectively. The hypsochromic shift for PBN-3 (λ_{647}) than the corresponding PBN-1 (λ_{668}) was probably due to the stronger interaction of functionalized alkoxysilane to the PB inner surface at a nanometer scale. It justifying that inclusion of appropriate EETMSi content alters charge transfer transition spectra by affecting the columbic energy expended in transferring the localized electrons from (+II) Fe-C →N-Fe (+III) octahedral hole beside of modifying their particle dimension (Einaga et al., 1999). As the size of particles decreases, a lowering in confining dimension makes the energy levels discrete which widen up the band gap and inturn to its energy and ultimately causes shifting in absorption maxima ($E= hc/\lambda_{max}$) where, E=band gap energy and λ_{max}=absorption maxima (Kelly et al., 2003; Reguera et al., 2007)..

2.3.3 FTIR spectrum of PBN

A single and sharp band, shown at 2080 cm^{-1} corresponds to characteristics CN stretching vibrational mode of PB (Ayers and Waggoner, 1971). The intense and broad absorption band at 3440 cm^{-1} and 1620 cm^{-1} assigned to the OH stretching and H_2O bending modes of the interstitial water molecules respectively (Fig. 2.10 and Fig. 2.11A) in PB lattice (Qiu et al., 2007). The IR-spectra also contain a bands at 1764 cm^{-1} attributed to the carbonyl group while the shoulder peak at 1724 cm^{-1} assignable to an ester linkage (Fig. 2.10 and Fig. 2.11B), confirms the decomposition of THF-HPO to γ-butyrolactone (by-product) (McDermott, 1986; Stenberg et al., 1970). The absence of peak for an epoxy ring (1190 cm^{-1}, 891 cm^{-1}) in a spectrum and emersion of new peak at 1642 for alkene derivative (byproduct) interpreted the active participation of EETMSi (Fig. 2.10 andFig. 2.11C) during PBN formation (Pandey and Shukla, 2016). Table 2.1 listed with different band frequencies assigned to possible functional moiety in PBN, THF-HPO, and EETMSi.

2.3.4 Chemical approach of EETMSi and THF-HPO during PBN fabrication

It is noteworthy that EETMSi inclusion played a dramatic role in PBN preparation. THF-HPO alone took a comparatively long time (12-14 hours) during nanoparticle synthesis onward forming the larger ones (40-50 nm) (Pandey and Pandey, 2014). While, EETMSi apart failed to convert potassium ferricyanide into PBN in the absence of THF-HPO. It

was suggested that THF-HPO provides a medium to enables the ferricyanide complex dissociation to furnish free ferric ion (Fe^{3+}). Furthermore, EETMSi facilitates their rapid reduction to Fe^{2+} in collaboration with THF-HPO. Opening of the epoxy ring of EETMSi provides the residual ionic surfactants that probably anchor on a growing nanoparticles inner surface (Camargo et al., 2015).

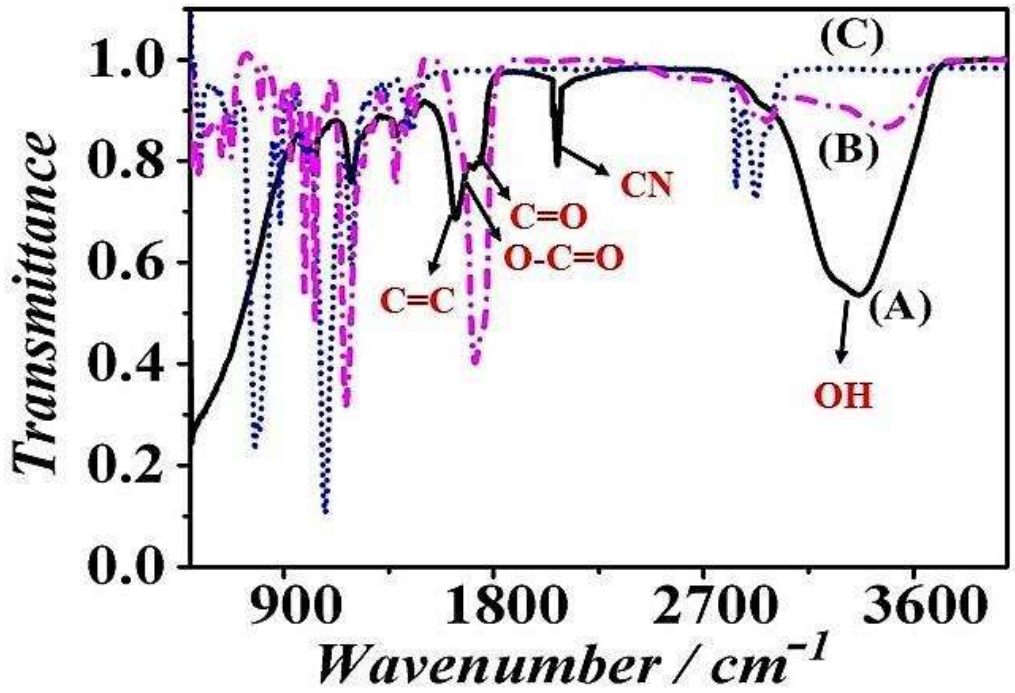

Figure 2.10: FTIR analysis of as-synthesized PBN (A) with THF-HPO (B), and EETMSi (C) through ATR.

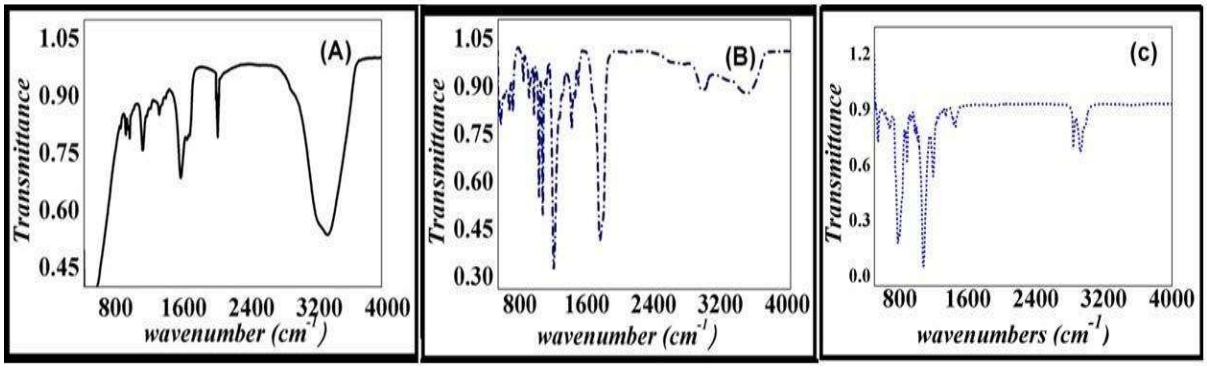

Figure 2.11: FTIR spectrum of as-synthesized PBN (A), THF-HPO (B), and EETMSi (C).

Table 2.1: F T IR data listed with assigned possible functional groups.

Band Assignment (cm^{-1})	Functional group	Refrences
3340	O—— H Str	(Qiu et al., 2007)
2080	C≡≡N Str	(Ayers and Waggoner, 1971)
1766	C═O Str	(McDermott, 1986; Stenberg et al., 1970)
1720	O C O	(McDermott, 1986; Stenberg et al., 1970)
1642	C C	(Pandey and Shukla, 2016)
1086	Si O	(Pandey and Shukla, 2016)
1615	H_2O bend	(Qiu et al., 2007)

2.3.5 Stability and solubility of nanoparticle

Insolubility of bulk PB in organic media limits its practical applicability as a functional materials. The PBN, mediated through EETMSi and THF-HPO are well-dispersed in various organic solvents as shown in Fig 2.12. It is noteworthy that alkoxysilane functionalized PBN species are easily peptized as the blue colloidal sol in organic solvents and possessing the nanoscopic size and functionalized hydrophobic alkoxy group on the surface of PB that lower the energy at electrical double layer to enhance the solublity and stability of colloidal sol.

2.3.6 Electrochemical behavior of PBN

Cyclic voltammetry of PBN-modified electrode has been recorded in 0.1 M KNO_3 solution at the scan rate of 5 mV/s vs. Ag/AgCl. It comprises the voltammograms for graphite paste electrodes modified with different sized PB colloids, i.e., PBN-1, PBN-2 and PBN-3(Fig. 2.13(A,B,C)) respectively revealing two reversible redox peaks. The redox couple at lower potential (0.2 V) correspond to the oxidation of PW to PB and reduction of BGto PW, and another at higher (0.9 V) owing to PB oxidation to BG (PY) and reduction of PY to PB with potassium ion as the counter ion (Farah et al., 2013). As can be seen,

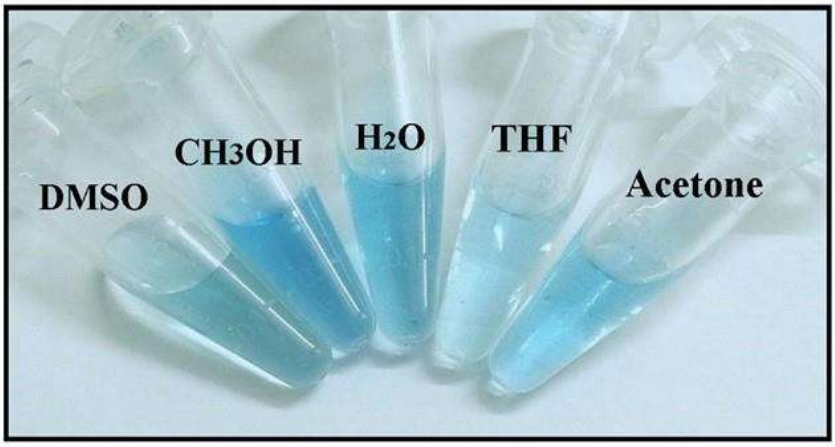

Figure 2.12: Dispersibility of as-synthesized PBN in different solvents.

there is a gradual increase in peak currents density with the decrease in nanoparticle size. The different peak separation potential (Ep = Epa - Epc) ranged from 15 to 22 mV (close to 0 mV) unveil an adsorbed electroactive species on the electrode surface. The PB/PW redox peak sharpness define the nanomaterial quality with facile electron transfer and indicating their surface dependent redox activity (Ellis et al., 1981).

2.3.7 Electrochemical sensing of H_2O_2

The H_2O_2 sensing with high sensitivity and selectivity over low potential is a crucial point (Karyakin and Karyakina, 1999). Electrocatalytic reduction of H_2O_2 over PB modified electrode surface was performed in PBS buffer (0.1 M, pH~ 6.85) containing 0.1 M KCl as supporting electrolyte. Fig. 2.14(A,B,C) depicts the cyclic voltammetry of PBN-1, PBN-2, and PBN-3 modified electrode in the absence (i) and the presence (ii) of H_2O_2(5 mM) at 10 mV scan rate. It was demonstrating that PBN exhibited size dependent electrocatalytic activity concerning onset potential and current response. Smaller-sized (PBN-3) display remarkable electrocatalytic response towards H_2O_2 reduction relative to PBN-1 (large-sized) and PBN-2 (medium-sized). It concludes that indeed smaller size PBN-3 provide the higher surface area for analyte species to get effectively adsorbed ona surface of it and even facilitate faster electron transfer (Sheng et al., 2015).

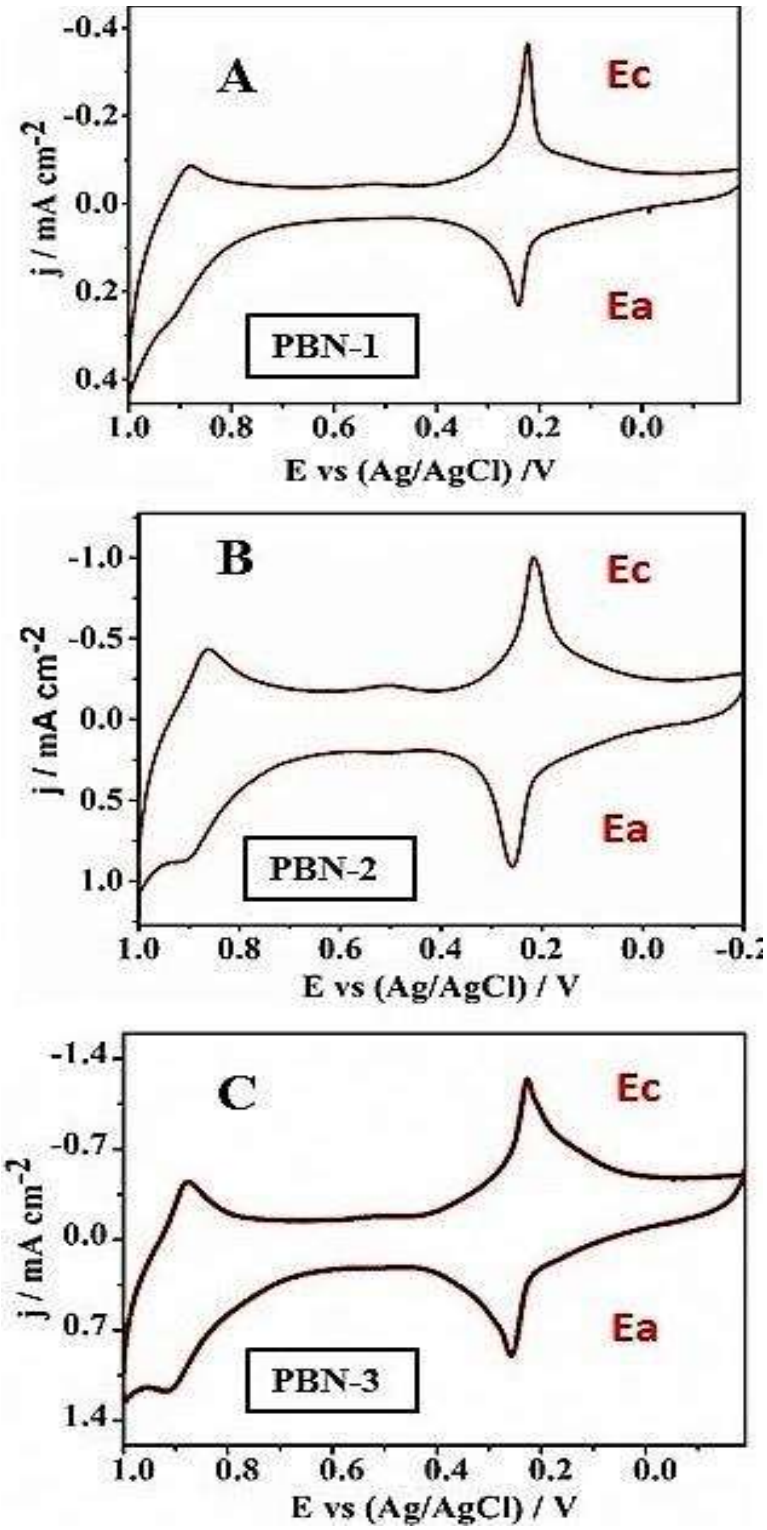

Figure 2.13: Study of electrochemical nature of PBN-1 (A), PBN-2 (B), and PBN-3 (C) modified electrodes in 0.1 M phosphate buffer (pH 7.0) at the scan rate of 5 mV/s.

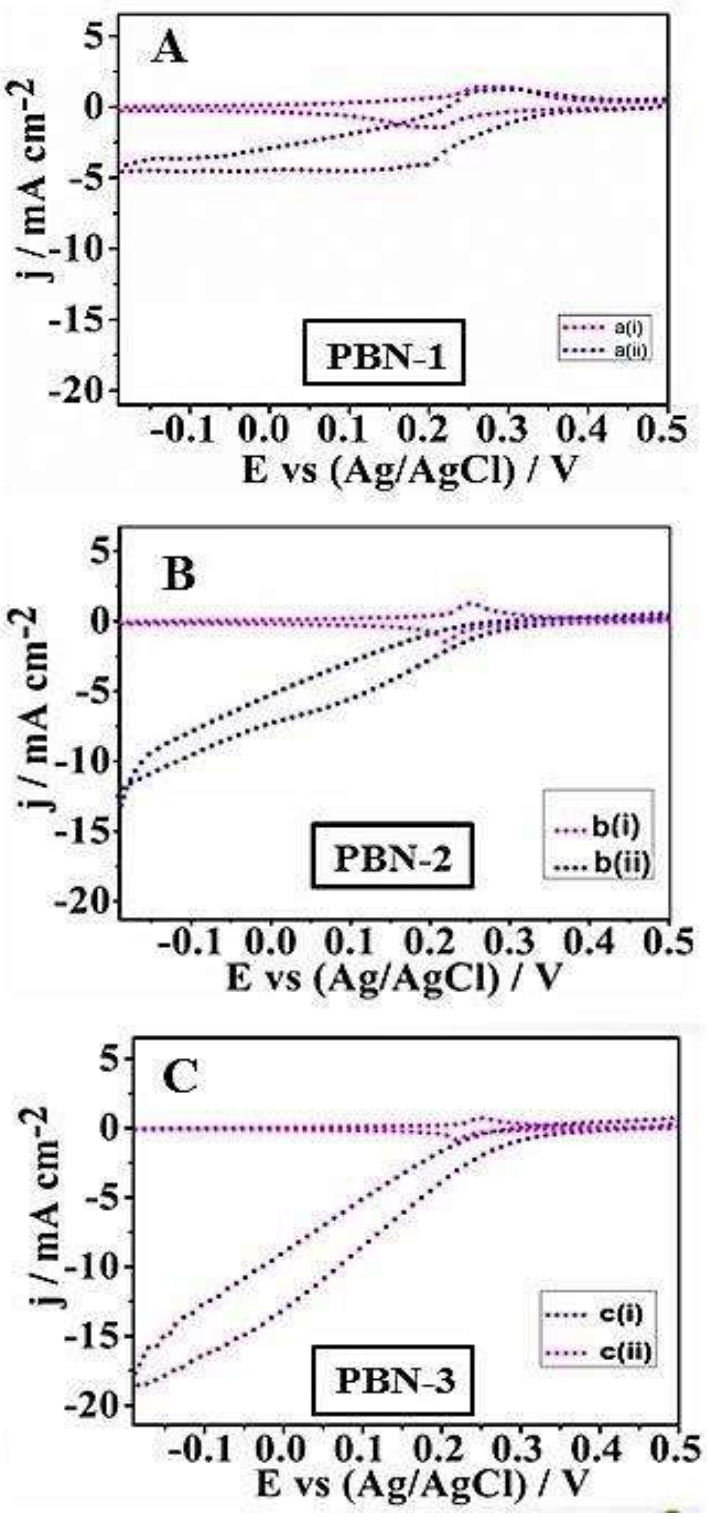

Figure 2.14: Cyclic voltammograms of PBN-1 (A), PBN-2 (B), and PBN-3 (C) modified systems in the absence (i) and presence (ii) of 1 mM H_2O_2 in 0.1 M phosphate buffer (pH-7.0) containing 0.5 M KCl .

Table 2.2: Kinetic parameters (K_m and V_{max}) justifying peroxidase like activity of various catalysts.

System	K_m/mM	V_{max}/Ms^{-1}	Refrences
Fe_3O_4 nanoparticle	154	9.78×10^{-8}	Ref Gao et al. (2007)
PB/y-Fe_2O_3	323.6	1.17×10^{-6}	Ref Zhang et al. (2010b)
FeHCF	9.038	8.40×10^{-7}	Ref Pandey and Pandey (2013b)
Mn-FeHCF	5.64	8.69×10^{-7}	Ref Pandey and Pandey (2013b)
PB-Ferritin	11.984	7.20×10^{-7}	Ref Zhang et al. (2013)
HRP	3.7	8.71×10^{-8}	Ref Gao et al. (2007)
PBN-1	1.5	8.30×10^{-7}	This work (Fig.2.17(*A*))
PBN-2	1.18	9.80×10^{-7}	This work (Fig.2.17(*B*))
PBN-3	0.9	13.00×10^{-7}	This work (Fig.2.17(*C*))

2.3.8 Peroxidase mimetic activity of PBN

The peroxidase mimetic activity of as synthesized PBN was estimated spectrophotometrically during catalytic oxidation of chromogenic peroxidase substrate o-dianisidine using H_2O_2. The appearance of brown colour resultant into an absorption maxima at 430 nm (Fig. 2.15(A,B,C)) in UV-Vis spectrum characterizing o-dianisidine oxidation, justifying enzyme like ability of as prepared PBN. However, PBN mimetic ability towards peroxide has been evaluated based on kinetic data recorded in time scan mode at 430 nm in the presence of varying concentrations of H_2O_2 (Fig. 2.16(A,B,C)) and fixed concentration of o-dianisidine using PBN of different size in phosphate buffer (0.1 M, pH 7.0). The results revealed the faster kinetic ability of PBN-3 as compared to PBN-1 and PBN-2 (Fig. 2.16). K_m values for as fabricated PBN was evaluated from Michaelis-Menton curves as shown in Fig. 2.17(A,B,C). Size dependent K_m and V_{max} for PBN was deliberated and has been listed in Table. 2.2 which indicates better kinetic activity of PBN-3.

2.3.9 Development of PBN encapsulated silica-alginate beads

Although, the immobilization of active materials into the Ca-alginate beads proved to be

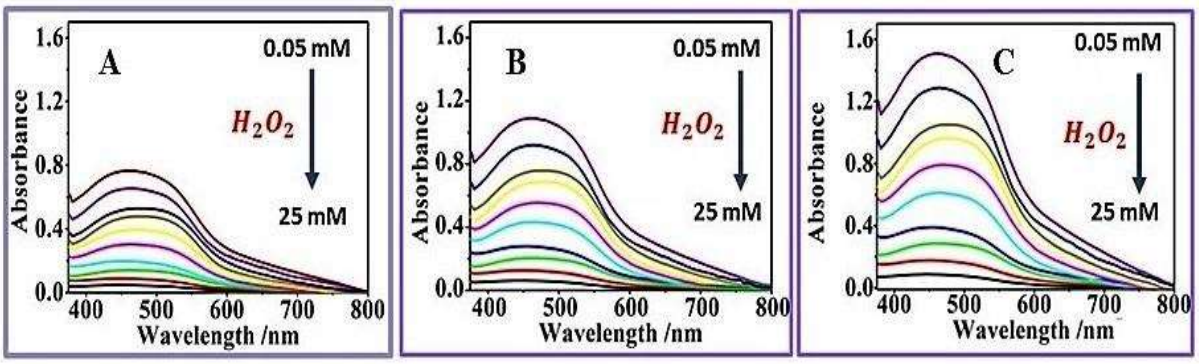

Figure 2.15: UV-Vis spectra of o-dianisidine-H_2O_2-PBN system displaying change in absorbance as a function of H_2O_2 concentration variations catalyzed by PBN-1 (A), PBN-2 (B), and PBN-3 (C).

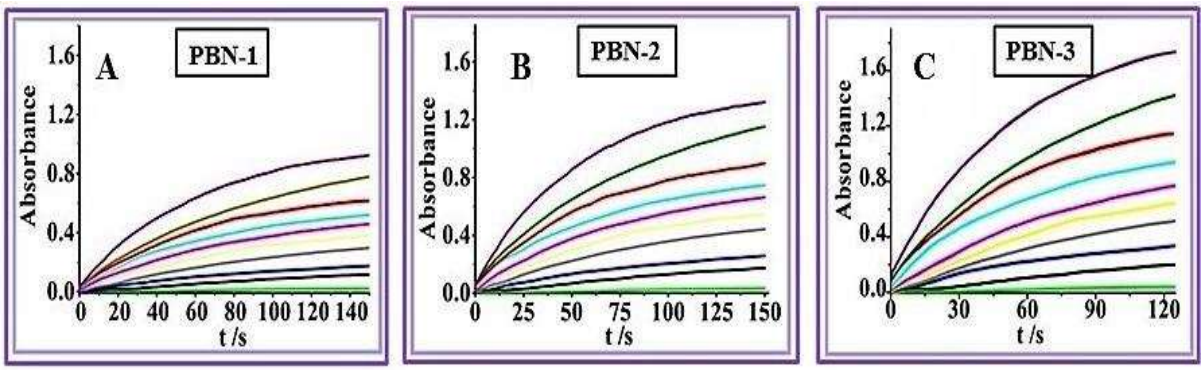

Figure 2.16: Time dependent absorbance changes at 430 nm in the presence of different concentration (0.05 to 25 mM) of H_2O_2 and fixed concentration of o-dianisidine (50 μM) catalyzed by PBN-1 (A), PBN-2 (B), and PBN-3 (C) respectively.

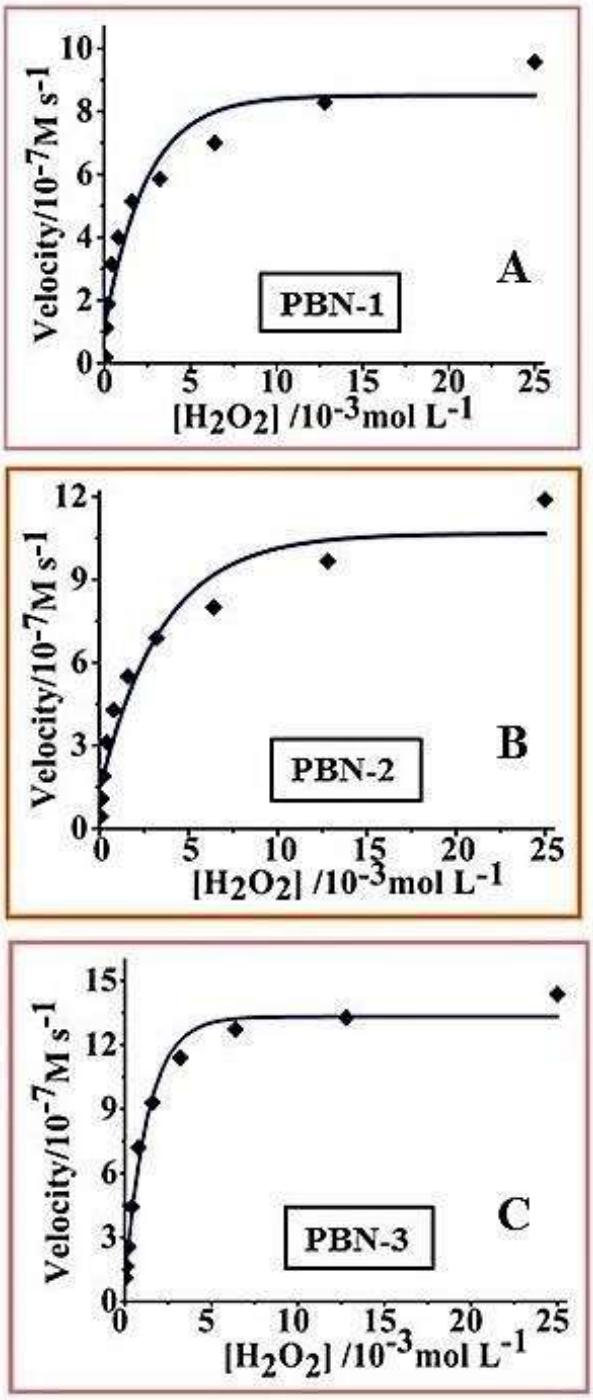

Figure 2.17: Kinetic analysis of PBN-1 (A), PBN-2 (B), and PBN-3 (C) with H_2O_2 as a substrate.

cost-effective. However, there is a possibility of leaching out of smaller nanomaterial from relatively larger pores. The pore sizes of such gel beads are not compatible with retaining the nanoscale materials lying between 1-16 nm, which limits their operational activity over the time. Accordingly, specific properties of the alkoxy group, that allow the formation of -Si-O-Si- linkages within alginate matrix, are explored to control the pore size through sol-gel processing and lead to the encapsulation of PBN-1, PBN-2 and PBN-3. The SEM micrographs of calcium alginate bead, synthesized in the absence of EETMSi, has been shown in Fig. 2.18(A). While Fig. 2.18(B) and Fig. 2.18(C) depicts the SEM image of EETMSi modified silica-alginate bead and fabricated PB-encapsulated silica-alginate bead respectively. Fig. 2.18(D) show the SEM images of only PBN-3. These images predict controlled porous morphology with encapsulated PBN within its matrix. The strong peak observed in the EDX spectrum (Fig. 2.19) confirmed the presence of all mandatory elements such as C, N, O, Si, Ca and Fe and approved similarly the individuality of PBN within silica-alginate bead. The prepared nanoparticles-encapsulated bead system revealed the weight percentage at 19.24 % of C, 10.16 % of N, 27.40 % of O, 4.47 % of Si, 34.09 % of Ca and 4.63 % of Fe in the EDX spectrum for the corresponding sample. The developed beads have also shown the great potentiality to enclose other nanoparticles like palladium and active enzyme for specific applications.

2.3.10 Electrochemical sensing of pyrogallol using PBN encapsulated silica-alginate beads

The role of PBN-encapsulated silica-alginate beads has been evaluated in electrochemical sensing. However, the PBN-encapsulated silica-alginate beads are difficult to be placed at the surface of the electrode. Accordingly, electrochemical sensing of pyrogallol in the bulk reaction system was examined by differential pulse voltammetry at the surface of the graphite paste electrode in 0.1 M PBS (pH$\sim$ 6.8). The differential pulse voltammogram (DPV) of pyrogallol, as recorded in the absence of PBN-encapsulated beads, revealed a peak near to 0.45 V justify direct-oxidation of analytes as shown in Fig. 2.20A. To obtain more insight into pyrogallol oxidation, the differential pulse voltammogram (DPV) analysis was performed under different conditions containing; (i) with H_2O_2, and (ii) with H_2O_2 in the presence of PBN-encapsulated silica-alginate beads. The outcomes have been shown in Fig. 2.21A and Fig. 2.22A respectively. The redox peak centered at near to 0.45

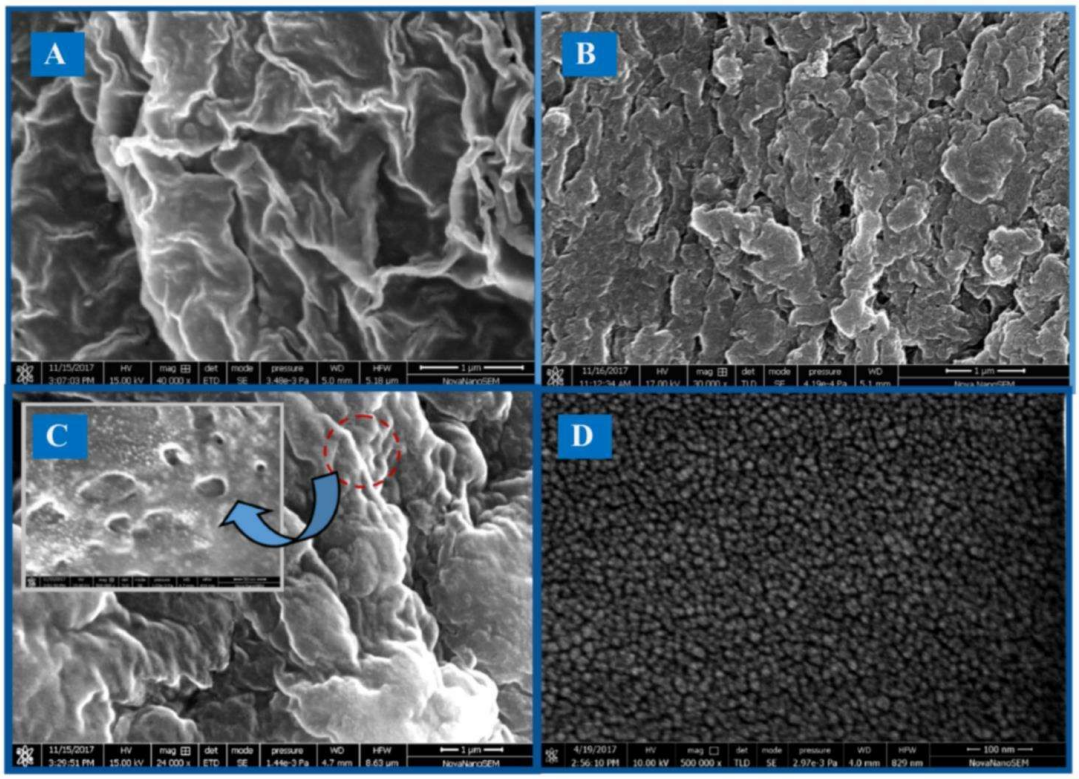

Figure 2.18: SEM images of calcium-alginate bead (A), silica-alginate bead (B), PBN-encapsulated silica-alginate bead (C), and PBN-3 (D).

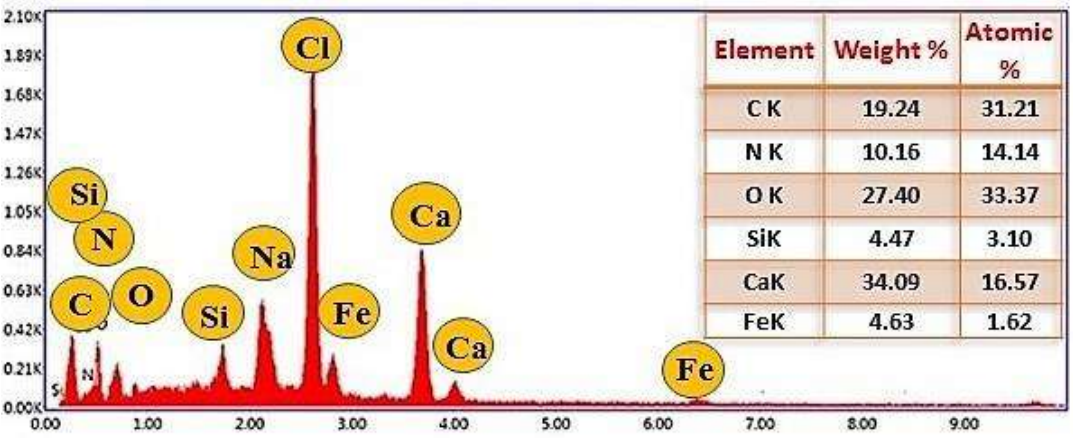

Element	Weight %	Atomic %
C K	19.24	31.21
N K	10.16	14.14
O K	27.40	33.37
SiK	4.47	3.10
CaK	34.09	16.57
FeK	4.63	1.62

Figure 2.19: EDX spectra of PBN-encapsulated silica-alginate beads identify the presence of all elemental species.

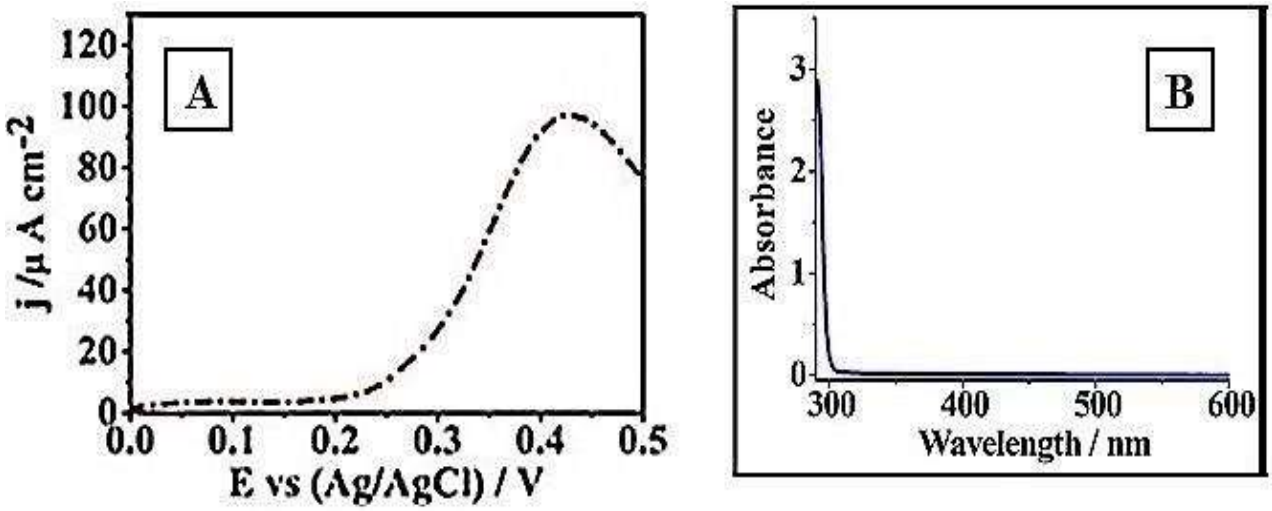

Figure 2.20: Differential pulse voltammogram justifying auto-oxidation of pyrogallol individually (A) in 0.1 M phosphate buffer (pH-7.0) containing 0.5 M KCl. UV-Vis spectrum of the resultant system (B).

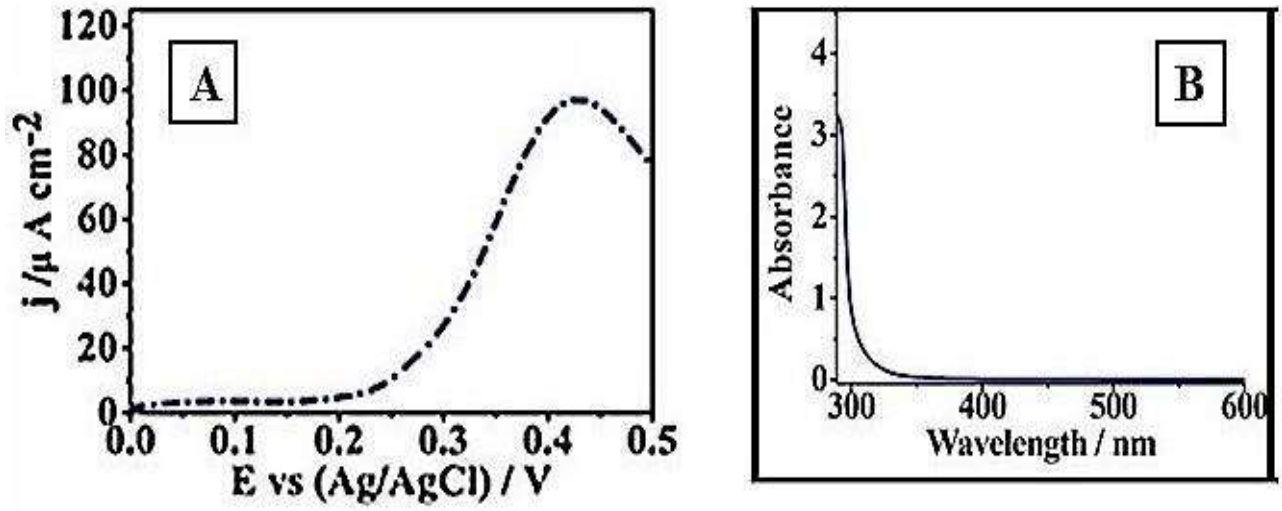

Figure 2.21: Differential pulse voltammogram justifying auto-oxidation of pyrogallol, in the presence of H_2O_2 (A) in 0.1 M phosphate buffer (pH-7.0) containing 0.5 M KCl. And UV-Vis spectrum of the resultant system (B).

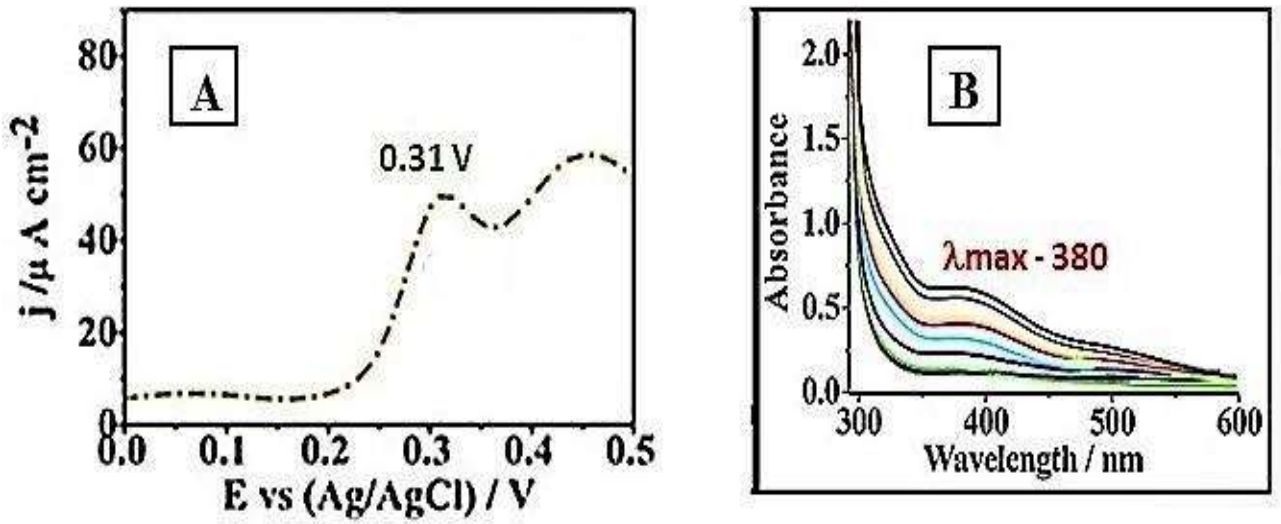

Figure 2.22: Differential pulse voltammogram justifying auto-oxidation of pyrogallol, in the presence of H_2O_2 and PB-encapsulated silica-alginate beads (A) in 0.1 M phosphate buffer (pH-7.0) containing 0.5 M KCl. The UV-Vis spectrum of resultant system displaying increase in absorption maxima as function of pyrogallol concentration (B).

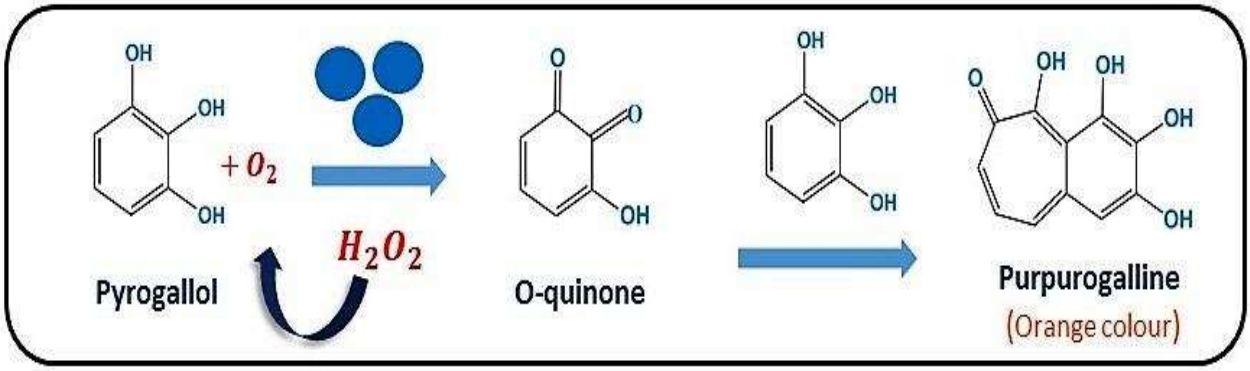

Figure 2.23: Plausible mechanism of Pyrogallol oxidation to purpurogallin via PB-encapsulated silica-alginate beads with H_2O_2. (Where ● represent PB-encapsulated silica-alginate beads).

V in DPV correspond to the auto-oxidation of pyrogallol at the electrode surface. The finding demonstrates that the addition of H_2O_2 did not cause any change in the redox peak (as shown in Fig. 2.21A) and was inefficient to converting pyrogallol into reaction products. However, the presence of H_2O_2 along with PBN-encapsulated silica-alginate beads initiate the significant amplification in electrochemical sensing as shown in Fig. 2.22(A).

The finding discussed above deal with the introduction of a new peak at 0.3 V vs. Ag/AgCl in DPV curve, justifying selectivity in pyrogallol sensing. It is essential to account the function of PB, in generating selectivity present in the bulk of the reaction system instead of the electrochemical interface. The catalytic process indicates the formation of purpurogallin, having absorption peak in visible region of spectrum as shown in Fig. 2.22(B). While, the formation of hydroxysilanequinone is not observed when the PB-encapsulated bead is absent in reaction mixture (Fig. 2.20B and Fig. 2.21B). The hydroxyquinoline is relatively better electroactive and may undergo natural oxidation as compared to pyrogallol thus introducing selectivity in electrochemical sensing. These PBN-encapsulated bead act as an efficient catalyst during the transformation of pyrogallol into electroactive hydroxyquinone species and justifying the role of as prepared nanomaterial towards selective electrochemical sensing of pyrogallol. It was concluded that hydroxyquinoline undergoes rearrangement and coupled to pyrogallol molecule (colourless) to produce purpurogallin (dark yellow) as shown in Fig. 2.23 (Tauber, 1953). A proposed mechanism has been shown in Fig. 2.24 disclose how PBN-silica-alginate bead catalyze the coupled oxidation with H_2O_2 and authenticate their intrinsic peroxidase-like activity towards a pyrogallol substrate.

2.4 CONCLUSION

In summary, we have succeeded in reporting a simple and flexible chemical technique for PBN synthesis of different sizes using a single precursor. The dimension of PBN could be finely achieved by employing the desired alkoxysilanes (EETMSi) content. The EETMSi emerged as a promising finding during an investigation that controls PBN size followed by stabilizing it via resultant hydrophobic reaction product and enhanced its dispersibility in

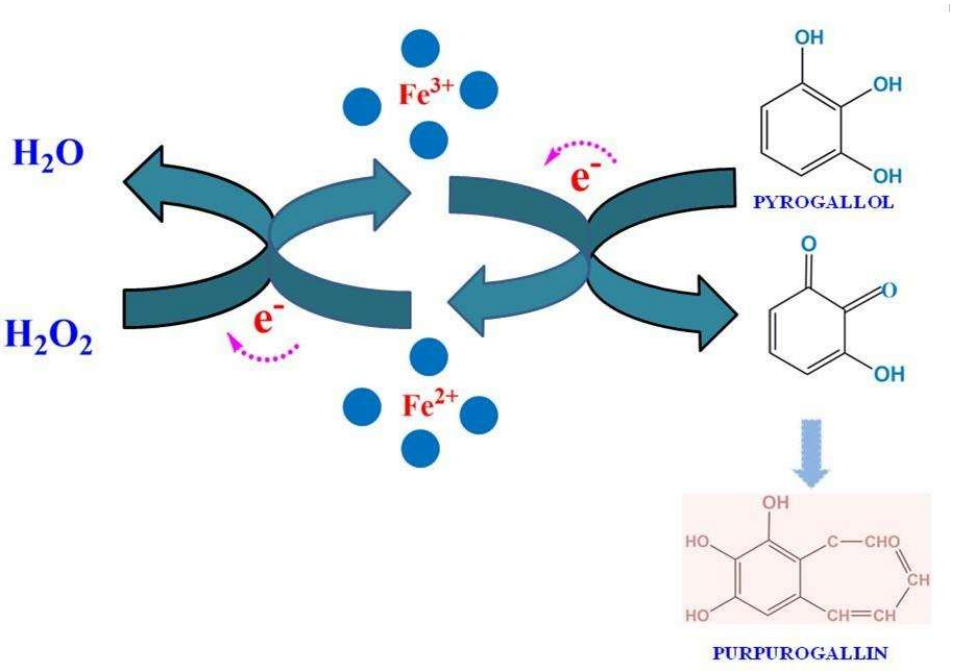

Figure 2.24: Catalytic oxidation of pyrogallol to purpurogallin through PBN doped silica-alginate bead.

---

both aqueous and various organic solvent. Non-aggregation and well-salvation have also been observed. The experimental result also displays the perfect intrinsic peroxidase-like activity of these nanomaterials, and size-dependent catalytic efficiencies towards H_2O_2 at PBN modified electrode. Consequently, EETMSi concentration remarkably affects the charge transfer complexion and leads to attractive size-dependent properties based on the organic-inorganic ratio at a nanometer scale. High stability and intrinsic peroxidase activity authenticate the above synthesized PBN as superior artificial peroxidase. The resulting alkoxysilanes mediated PBN was homogeneous with alginic acid and appropriate for developing beads of controlled porosity. These fabricated beads demonstrate the selective oxidation of pyrogallol in the presence of H_2O_2. Further, alginate beads add valuable information as the mesoporous matrix of silica-alginate could loaded with another suitable reagent and worthy for various applications.